1998

Theoretical Analysis of Metal Hydride Electrodes: Studies on Equilibrium Potential and Exchange Current Density

Bala S. Haran
University of South Carolina - Columbia

Branko N. Popov
University of South Carolina - Columbia, popov@engr.sc.edu

Ralph E. White
University of South Carolina - Columbia, white@cec.sc.edu

Publication Info

Journal of the Electrochemical Society, 1998, pages 4082-4090.

Publisher's link: http://dx.doi.org/10.1149/1.1838918
DOI: 10.1149/1.1838918

Theoretical Analysis of Metal Hydride Electrodes

Studies on Equilibrium Potential and Exchange Current Density

Bala S. Haran,* Branko N. Popov,* and Ralph E. White*

Department of Chemical Engineering, University of South Carolina, Columbia, South Carolina 29208, USA

ABSTRACT

A theoretical model for the metal hydride electrode has been developed assuming that hydrogen diffusion in the alloy and charge-transfer at the surface control the discharge process. Theoretical equations for the dependence of equilibrium potential and exchange current density on the surface hydrogen concentration have been derived. These parameters have been used to correlate experimental data with the theoretical electrode discharge model. Analysis of both the experimental and theoretical discharge curves reveals a potential plateau determined by the magnitude of the interactions between the hydrogen in the alloy and the unhydrided metal. Neglecting these hydrogen-metal site interactions results in simulations predicting the electrode potential varying over the entire duration of discharge. The results also indicate that utilization of the electrode is controlled by the rate of hydrogen diffusion in the electrode and by the alloy particle size. Kinetic resistance at the surface is a determining factor of the polarization losses of the electrode. The variation of equilibrium potential and exchange current density with the state of charge has been characterized experimentally. These results are compared with the model predictions, and good agreement is seen.

Introduction

Metal hydrides (MH) are rapidly replacing cadmium as the negative electrode in conventional Ni-Cd battery systems.[1-3] This has led to a tremendous increase in research on the application of intermetallic hydrides as anodes for energy-conversion applications.[2] The main factors affecting the performance of metal hydride electrodes are capacity, cycle life, and power density of the negative electrode. These factors are determined by both the kinetics of the processes occurring at the metal-electrolyte interface and the rate of hydrogen diffusion within the bulk of the alloy. Electrode parameters such as the exchange current density are a measure of the electrocatalytic activity of the alloy and therefore control the physical processes occurring at the interface and in the bulk of the electrode.[3] This gives rise to the need to understand and predict the performance of these alloys as electrodes.

Although many authors have presented different models for the nucleation and phase transformation processes occurring during gas-phase hydriding, there are few models which describe the metal hydride as an electrode.[4-11] Also, these models do not consider the critical interactions between the hydrogen absorbed in the lattice and the unhydrided metal alloy. Experimental discharge curves of metal hydrides reveal a potential plateau during the major duration of discharge. However, neglecting the nonidealities arising due to the hydrogen-metal site interactions results in simulations of the discharge curves which differ sharply from the actual experimental data.

Furthermore, electrochemical characterization and hence comparison of different alloys as negative electrodes for Ni-MH cells involves measurement of the exchange current density and equilibrium potential as a function of electrode state of charge (SOC). Yayama et al.[12,13] derived expressions for the equilibrium potential and the exchange current density of the hydride electrode but neglected nonidealities in the activity coefficients because of changes in the excess free energy during discharge.[14] Characterizing changes in the hydride equilibrium potential and exchange current density is critical not only for evaluating different MH alloys but also for developing a fundamental understanding of the mechanism of hydride electrodes. Furthermore, the kinetic and thermodynamic equations developed herein could be part of larger battery models (De Vidts et al.[11] and Paxton and Newman[7]) essential for the design and optimization of metal hydride cells.

The objective of our effort is to describe mathematically the shortcomings outlined above and to incorporate them in the discharge model. In the first part of this paper, we develop a model for the discharge of the metal hydride electrode under a constant applied current and solve for the concentration profile of hydrogen in the alloy particle. The performance of the hydride electrode under galvanostatic conditions is simulated assuming that only hydrogen diffusion and charge transfer contribute to the polarization losses of the electrode. The Butler-Volmer equation for the hydride electrode is derived taking into account the hydrogen-metal site interactions in the alloy. A Margules symmetrical expression is used to account for changes in the activity coefficient with concentration of hydrogen. A theoretical formalism has been developed to evaluate the equilibrium potential and the exchange current density as a function of state of charge of the electrode. These parameters have been used to correlate experimental discharge data with the theoretical electrode discharge model. We then examine the effects of the reaction and subsequent diffusion of hydrogen inside the particle on the electrode performance.

Model Development

The metal hydride electrode shown in Fig. 1 is modeled in this work. The cylindrical hydride electrode is filled with spherical alloy particles that are in close contact with each other. The particles are in contact with a current collector at the top and one at the bottom of the pellet electrode. The void volume of the electrode is filled with the electrolyte, namely, concentrated potassium hydroxide solution. In order to simplify the analysis, we consider here only the most important physical phenomena. Consequently, only a single spherical hydride particle is taken into account, and we consider the reaction and one-dimensional transport of hydrogen through the particle. The ohmic polarization due to changes in the concentration of electrolyte and the particle-to-particle contact resistance have not been considered. For a thin hydride electrode, the ohmic drop, and the mass-transfer resistance in the electrolyte can be neglected. The reaction at the electrolyte/particle interface is characterized by the exchange current density and the equilibrium potential of the electrode. These parameters are dependent on the hydrogen concentration and are treated as such in the model. A macroscopic approach, with the spherical diffusion equation and dilute solution theory, has been used to model the transport of hydrogen through the particle.

The electrode reaction at the surface of the hydride particle is

$$MH_{x,ads} + xOH^- \underset{\text{charge}}{\overset{\text{discharge}}{\rightleftharpoons}} M + xH_2O + xe^- \qquad [I]$$

During discharge, hydrogen atoms desorb in this charge-transfer step, and electrons are supplied to an external circuit. Due to the gradient in concentration between the

* Electrochemical Society Active Member.

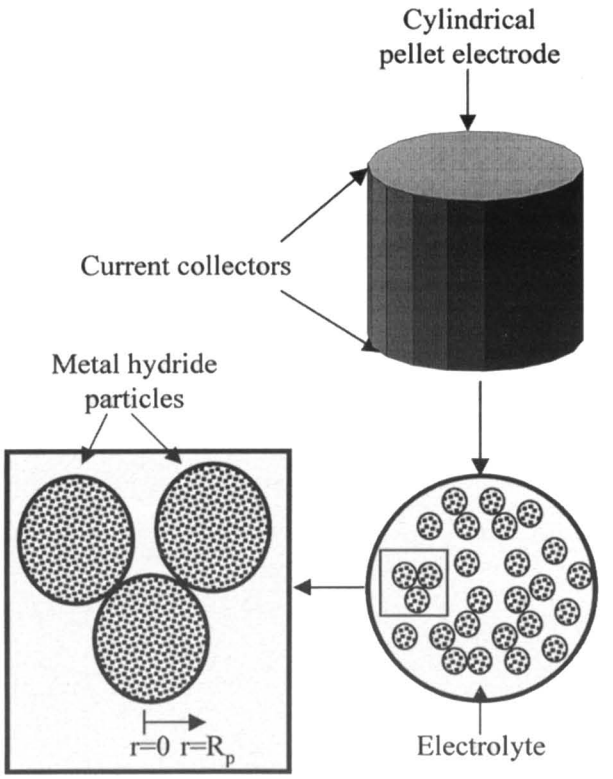

Fig. 1. Schematic diagram of the pellet electrode modeled. The metal hydride particles are immersed in a pool of 6 M KOH electrolyte. The hydrogen in the particle reacts electrochemically with the hydroxide ions at the electrolyte/particle interface.

bulk and the surface of the particle, the absorbed hydrogen atoms diffuse toward the surface of the alloy

$$MH_{x,abs}^{bulk} \rightleftarrows MH_{x,ads}^{surface} \qquad [II]$$

Zhang et al.[15] have modeled the transient uptake of hydrogen by metal alloy particles using a shrinking-core model. Assuming a constant concentration of hydrogen at the particle/electrolyte interface a semianalytical solution has been derived for the fractional conversion of hydrogen. In this work we do not differentiate between the α-β transitions that occur during hydriding/dehydriding of the interior metal alloy. However, we focus on the changes in the hydrogen concentration at the particle-electrolyte interface due to the electrochemical reaction I. We also study the effect of these changes on the electrode discharge voltage and equilibrium potential.

During charge, the reverse of the processes described above happens, beginning with the hydrogen adsorption at the metal particle surface. This results in hydrogen absorption as given by the reverse of reaction I with the flux of hydrogen atoms toward the interior of the alloy particle from the surface. For a constant discharge current, it is of interest to simulate the active material potential (Φ) at different electrodes states of charge. In order to predict this, the hydrogen concentration at the surface of the particle is needed as a function of time. To determine the surface hydrogen concentration for a galvanostatic charge/discharge, the concentration profile of hydrogen is first obtained by solving the one-dimensional time-dependent diffusion equation for the spherical particle

$$\frac{\partial c}{\partial t} = \frac{D}{r^2}\frac{\partial}{\partial r}\left(r^2\frac{\partial c}{\partial r}\right) \qquad [1]$$

where D is the diffusion coefficient of hydrogen which is assumed not to vary with the state of charge. The initial concentration of hydrogen is assumed to be uniform throughout the particle. From symmetry, the hydrogen concentration gradient is zero at the center of the particle ($r = 0$)

$$\text{at } t = 0,\ c = c^o \qquad [2]$$

$$\text{at } r = 0,\ \frac{\partial c}{\partial r} = 0 \qquad [3]$$

$$\text{at } r = R_p,\ D\frac{\partial c}{\partial r} = -\frac{j'}{F} \qquad [4]$$

The boundary condition at the interface arises from the relationship between the rate of diffusion of hydrogen to the surface of the hydride alloy and the current density at the particle/electrolyte interface ($r = R_p$). The local current density, j', represents the reaction rate at the particle/solution interface. This is related to the current per unit mass of the electrode, j expressed in A/g applied at the current collector, through the amount of material, w_{MH}, volume of the pellet, V, electrode porosity, ϵ, and the electroactive surface area per unit volume of the electrode, a_{MH}

$$j' = \frac{jw_{MW}}{a_{MH}V(1-\epsilon)} \qquad [5]$$

The electroactive surface area is calculated assuming that all the particles are spherical in shape, identical in size, and with their entire surface area exposed to the electrolyte. This leads to the expression[11]

$$a_{MH} = \frac{3(1-\epsilon)}{R_p} \qquad [6]$$

For a constant-current discharge solving Eq. 1 to 4 by means of Laplace transforms gives[16]

$$c = c^o - \frac{j'R_p}{FD}\left[\frac{3tD}{R_p^2} + \frac{1}{10}\left(5\frac{r^2}{R_p^2} - 3\right) - 2\frac{R_p}{r}\sum_{n=1}^{\infty}\frac{\sin\left(\frac{\lambda_n r}{R_p}\right)}{\lambda_n^2\sin(\lambda_n)}e^{-\frac{\lambda_n^2 tD}{R_p^2}}\right] \qquad [7]$$

Equation 7 can be written in dimensionless form as

$$\hat{c} = 1 - \delta\left[3\tau + \frac{1}{10}(5\hat{r}^2 - 3) - \frac{2}{\hat{r}}\sum_{n=1}^{\infty}\frac{\sin(\lambda_n\hat{r})}{\lambda_n^2\sin(\lambda_n)}e^{-\lambda_n^2\tau}\right] \qquad [8]$$

where δ, a dimensionless parameter, is given by

$$\delta = \frac{j'R_p}{Fc^oD} \qquad [9]$$

The parameter describes the relative contributions to the polarization losses from the reaction at the surface and the transport of hydrogen in the bulk of the alloy. Integration of the concentration in the particle given by Eq. 8 over the particle volume gives the average hydrogen concentration in the particle at any instant during the discharge of the pellet as

$$\bar{c} = 1 - 3\delta\tau \qquad [10]$$

where

$$\tau = \frac{tD}{R_p^2} \qquad [11]$$

The variable of interest, namely, the dimensionless surface concentration ($\hat{c}_s$), is obtained by substituting $\hat{r} = 1$ into Eq. 8

$$\hat{c}_s = 1 - \delta\left[3\tau + 0.2 - 2\sum_{n=1}^{\infty}\frac{1}{\lambda_n^2}e^{-\lambda_n^2\tau}\right] \qquad [12]$$

For long periods of discharge, the exponential term on the right can be neglected, and the surface concentration reduces to

$$\hat{c}_s = 1 - \delta[3\tau + 0.2] \qquad [13]$$

When the surface concentration drops to zero, the electrode has been completely discharged, and no further current can be drawn. Equation 12 can be rewritten to calculate the time for discharge, τ_d, for the metal hydride electrode under a constant applied current

$$\delta = \frac{1}{\left[3\tau_d + 0.2 - 2\sum_{n=1}^{\infty} \frac{1}{\lambda_n^2} e^{-\lambda_n^2 \tau_d}\right]} \quad [14]$$

For a given current per unit mass, j, Eq. 14 can be solved to obtain the time for discharge, τ_d. For long discharge periods the discharge time can be directly obtained from Eq. 13 as

$$\tau_d = \left(\frac{1}{\delta} - 0.2\right)\frac{1}{3} \quad [15]$$

The electrode utilization is then calculated as

$$U = \frac{j\tau_d R_p^2}{3600 Q_o D} \times 100\% \quad [16]$$

where Q_o is the actual capacity of the electrode.

Electrode kinetics and thermodynamics.—If the solution and solid-phase resistivities are negligible, the current density at the particle surface due to reaction I is a function of the concentration of hydrogen at the surface, the overpotential, and the number of free metal sites at the alloy/electrolyte interface. Under these conditions the current density given by the concentration-dependent Butler-Volmer equation is[11]

$$j' = Fk_+ \hat{a}_H^p e^{\beta f\Phi} - Fk_- \hat{a}_M^q e^{-(1-\beta)f\Phi} \quad [17]$$

where $\hat{a}_H$ is the activity of adsorbed hydrogen and $\hat{a}_M$ represents the empty sites on the particle surface. Since the activity of free metal sites and hydrogen are unknown quantities, we express them in terms of the activity coefficient and concentration as $a = \gamma c$. The potential difference at the particle interface, Φ, is a theoretical entity and hence cannot be measured experimentally. We define an electrode overpotential, η, at the particle/electrolyte interface relative to a reference potential as

$$\eta = \Phi - \Phi_{eq} \quad [18]$$

where Φ_{eq} denotes the potential difference at equilibrium. Rewriting Eq. 17 with these expressions for the activities, η, and also considering[11]

$$\hat{a}_M = (1 - \hat{c}_s)\gamma_M \quad [19]$$

we have

$$j' = Fk_+ \hat{c}_s^p \gamma_H e^{\beta f\Phi_{eq}} e^{\beta f\eta} - Fk_-(1 - \hat{c}_s)^q \gamma_M e^{-(1-\beta)f\Phi_{eq}} e^{-(1-\beta)f\eta} \quad [20]$$

where γ_M and γ_H are the free metal site and hydrogen activity coefficients, respectively. The hydride equilibrium potential is given by the activities of hydrogen and the free metal sites on the surface of the particle

$$\Phi_{eq} = \Phi^o - \frac{RT}{F}\ln\frac{\hat{a}_H}{\hat{a}_M} \quad [21]$$

A similar expression has been used previously[14] to account for the free interstitial sites needed for hydrogen absorption. However, previous treatments[12-14] of the hydride equilibrium potential and the exchange current density, have considered the activity coefficient to be a constant. Departures of γ from unity due to the interactions of the absorbed hydrogen in the metal lattice have been neglected. This approximation is true for ideal solutions or cases where the concentration of the active species does not vary significantly. However, intermetallic hydrides are nonideal solid solutions where the hydrogen content in the electrode varies over two orders of magnitude. Furthermore galvanostatic discharge curves for different hydride electrodes reveal a flat potential profile due to the interactions between the absorbed hydrogen and metal lattice. Neglect of the changes in γ would result in simulations predicting a potential varying significantly over the entire duration of discharge. Hence it is essential to consider the changes in the activity coefficient with concentration of the active species.

We account for the nonidealities in the activity coefficient by using a thermodynamic model that considers the changes in the free energy to be due to the interaction of absorbed hydrogen and the metal alloy. This approach is similar to that proposed for the nickel electrode by Barnard et al.[17] Verbrugge and Koch[18] used a similar approach for lithium intercalation in carbon fibers. A more detailed study in comparing different thermodynamic models for the variation in the activity coefficient has been done by Jain et al.[19] for the nickel electrode. Following the approach of Barnard et al.,[17] energy for the hydride electrode as the sum of (*i*) the free energy of reaction, G_R, (*ii*) free energy of mixing, G_I, and (*iii*) the excess free energy of interaction, G_E. We use the symmetric Margules expressions[17,19] for the variation of γ with concentration, namely

$$\ln\gamma_H = \frac{A}{RT}(1 - \hat{c}_s)^2 \quad [22]$$

and

$$\ln\gamma_M = \frac{A}{RT}\hat{c}_s^2 \quad [23]$$

where A is a constant. The total free energy is given by[17,19]

$$G_T = (1 - \hat{c}_s)\mu_H^o + \hat{c}_s\mu_H^o + RT\left[(1 - \hat{c}_s)\ln(1 - \hat{c}_s) + \hat{c}_s\ln\hat{c}_s\right] + A\hat{c}_s(1 - \hat{c}_s) \quad [24]$$

The electrode potential can be found from the differential of the total Gibb's free energy.[17] Differentiating Eq. 24 with respect to $\hat{c}_s$, we have the equilibrium potential of the hydride electrode as

$$\Phi_{eq} = \Phi^o - \frac{RT}{F}\ln\frac{\hat{c}_s}{(1 - \hat{c}_s)} + \frac{A}{F}[2\hat{c}_s - 1] \quad [25]$$

where

$$\Phi^o = \frac{(\mu_M^o - \mu_H^o)}{F} \quad [26]$$

The first and second terms in Eq. 25 represent, respectively, the reaction energy and the entropy contribution to the hydrogen potential. The third term represents the correction for the excess energy arising from the interactions due to hydrogen intercalation in the material. Φ^o represents the electrode equilibrium potential at 50% state of charge, i.e., $\hat{c}_s = 0.5$ in Eq. 25. Thus the electrode overpotential is given by substituting Eq. 25 into Eq. 18 as

$$\eta = \Phi - \Phi^o + \frac{RT}{F}\ln\frac{\hat{c}_s}{(1 - \hat{c}_s)} - \frac{A}{F}[2\hat{c}_s - 1] \quad [27]$$

Substituting Eq. 22, 23, and 25 into Eq. 20 we have

$$j' = Fk_+ \frac{\hat{c}_s^{p-\beta}}{(1 - \hat{c}_s)^{-\beta}} e^{\frac{pA}{RT}(1-\hat{c}_s)^2} e^{\beta f[\Phi^o + \frac{A}{F}(2\hat{c}_s - 1) + \eta]} - Fk_- \frac{(1 - \hat{c}_s)^{q-1+\beta}}{\hat{c}_s^{-(1-\beta)}} e^{\frac{qA}{RT}\hat{c}_s^2} \times e^{-(1-\beta)f[\Phi^o + \frac{A}{F}(2\hat{c}_s - 1) + \eta]} \quad [28]$$

At equilibrium both the forward and backward reactions proceed at the same rate, and the overpotential as well as the net current density are zero. Letting $\eta = 0$ and equating both terms in Eq. 28 leads to

$$e^{f\Phi^o} = \frac{k_-}{k_+}\hat{c}_s^{(1-p)}(1 - \hat{c}_s)^{(1-q)} e^{-\frac{A}{RT}[(2\hat{c}_s - 1) + p(1-\hat{c}_s)^2 - q\hat{c}_s^2]} \quad [29]$$

Substituting Eq. 29 into Eq. 28 gives

$$j' = Fk_+^{(1-\beta)}k_-^{\beta}\hat{c}_s^{p(1-\beta)}(1-\hat{c}_s)^{q\beta}e^{\frac{A}{RT}[p(1-\hat{c}_s)^2(1-\beta)+q\beta\hat{c}_s^2]}[e^{\beta f\eta} - e^{-(1-\beta)f\eta}] \quad [30]$$

Finally substituting the expression for the overpotential from Eq. 27 into Eq. 30 gives

$$j' = j_o\left[\frac{\hat{c}_s^{\beta}}{(1-\hat{c}_s)^{\beta}}e^{\beta f[\Phi-\Phi^o-\frac{A}{F}(2\hat{c}_s-1)]} - \frac{\hat{c}_s^{-(1-\beta)}}{(1-\hat{c}_s)^{-(1-\beta)}}e^{-(1-\beta)f[\Phi-\Phi^o-\frac{A}{F}(2\hat{c}_s-1)]}\right] \quad [31]$$

Equation 31 represents the modified form of the Butler-Volmer expression for the hydride electrode which takes into account the activity dependence of all parameters and also considers the interactions between the hydrogen and the metal lattice. The concentration dependent exchange current density, j_o is given by

$$j_o = j_{o,ref}\hat{c}_s^{p(1-\beta)}(1-\hat{c}_s)^{q\beta}e^{\frac{A}{RT}[p(1-\hat{c}_s)^2(1-\beta)+q\beta\hat{c}_s^2]} \quad [32]$$

where $j_{o,ref} = Fk_+^{(1-\beta)}k_-^{\beta}$ is calculated from the experimentally measured exchange current density at the reference state of 50% state of charge ($j_{0,50\%\ SOC}$ in A/g). In Eq. 32, when $\hat{c}_s = 0.5$ we have

$$j_{o,ref} = \frac{j_{o,50\%SOC}w_{MH}}{a_{MH}V(1-\epsilon)\left\{0.5^{p+\beta(q-p)}e^{\frac{0.5^2A}{RT}[p+\beta(q-p)]}\right\}} \quad [33]$$

Substituting for the normalized surface hydrogen concentration from Eq. 12 into Eq. 31 we get the electrode potential as a function of discharge time. We use a Newton-Raphson procedure to solve for the electrode potential, Φ (with respect to a Hg/HgO reference electrode) as a function of state of charge. The discharge time is related to the state of charge of the electrode by

$$SOC = 1 - \frac{jt}{3600Q_o} \quad [34]$$

At the end of discharge, a concentration gradient exists in the hydride particle favoring the transport of hydrogen from the bulk to the surface. Due to this hydrogen flux, the electrode potential changes and reaches a stable value only when the hydrogen concentration is the same throughout the particle. During experiments, the SOC studies were done once the electrode potential had stabilized. In such a case, the equilibrium potential and the exchange current density of the hydride electrode for reaction I are a function of the average hydrogen concentration, $\bar{c}$. For these cases, we substitute for $\bar{c}$ from Eq. 10 into Eq. 25 and Eq. 32 while evaluating Φ_{eq} and j_o, respectively. Table I lists the important equations derived for the hydride electrode.

Experimental

$LaNi_{4.27}Sn_{0.24}$ alloy was crushed and ground mechanically. The alloy was then plated with 25% by weight of nickel in an acid hypophosphite bath. A pellet electrode was prepared by mixing the encapsulated alloy with 2.5wt % polytetrafluoroethylene (PTFE) followed by hot pressing the material between two nickel meshes at 300°C and 500 MPa in a cylindrical press. A pellet of 0.8 cm diam, 0.9 mm thickness, and 450 mg by weight was obtained.

Characterization studies were done in a three-electrode setup. The working pellet electrode was inserted between two pieces of Plexiglas and immersed in a cell filled with 6 M KOH solution. All potentials are with respect to the Hg/HgO reference electrode. The counter electrode was a platinum mesh. The cell was maintained at a constant temperature of 25°C using a water bath. Bitrode Model LCN automated cycle-life tester was used for cycling the electrode. Electrochemical studies were done using the

Table I. Summary of equations derived for the hydride electrode.

$$\bar{c} = 1 - 3\delta\tau \quad [11]$$

$$\hat{c}_s = 1 - \delta\left[3\tau + 0.2 - 2\sum_{n=1}^{\infty}\frac{1}{\lambda_n^2}e^{-\lambda_n^2\tau}\right] \quad [12]$$

$$\Phi_{eq} = \Phi^o - \frac{RT}{F}\ln\frac{\hat{c}_s}{(1-\hat{c}_s)} + \frac{A}{F}[2\hat{c}_s - 1] \quad [25]$$

$$j' = j_o\left[\frac{\hat{c}_s^{\beta}}{(1-\hat{c}_s)^{\beta}}e^{\beta f[\Phi-\Phi^o-\frac{A}{F}(2\hat{c}_s-1)]} - \frac{\hat{c}_s^{-(1-\beta)}}{(1-\hat{c}_s)^{-(1-\beta)}}e^{-(1-\beta)f[\Phi-\Phi^o-\frac{A}{F}(2\hat{c}_s-1)]}\right] \quad [31]$$

$$j_o = j_{o,ref}\hat{c}_s^{p(1-\beta)}(1-\hat{c}_s)^{q\beta}e^{\frac{A}{RT}[p(1-\hat{c}_s)^2(1-\beta)+q\beta\hat{c}_s^2]} \quad [32]$$

model 352 SoftCorr System with EG&G Princeton Applied Research potentiostat/galvanostat model 273.

Initially the electrode was charged at a constant current of 6 mA for 10 h and then discharged at 3 mA until the potential reached a cutoff value of −0.6 V. These charge-discharge cycles were repeated ten times in order to condition the electrode. After activation of the electrode, SOC studies were performed to determine the electrode characteristics. Here, the SOC is defined with respect to the total useful capacity, determined from the time taken for discharge at a constant rate of 24 mA/g. The active material was discharged for a fixed time at a constant current, and the SOC was determined from the ratio of the time discharged to the time required for complete discharge. Once the alloy was discharged to a particular SOC, the electrode was left on open circuit until a stable potential was observed (typically between 45 to 60 min). After the potential stabilized, polarization studies were performed. The SOC studies were repeated until the electrode was discharged to its cutoff potential of −0.6 V. The ratio D/R_p^2 was determined from a galvanostatic discharge technique.[20] The parameters used in all the simulations are given in Table II.

Results and Discussion

Concentration profiles.—In order to understand the discharge process, Fig. 2a presents the hydrogen concentration in the particle at different times of discharge for the parameters given in Table II. For all times, the hydrogen concentration decreases from the center of the alloy ($r = 0$) toward the surface ($r = R_p$) where reaction I occurs. As the reaction proceeds, the hydrogen in the alloy gets progressively depleted. The hydrogen concentration gradient fuels further transport toward the surface. This results in a drop in concentration of hydrogen throughout the particle, from the center to the surface. The hydrogen concentration in the particle varies significantly as illustrated in Fig. 2b by the concentration profile after 5 h of discharge. The concentration at the center of the particle is significantly higher than the surface values. The concentration under-

Table II. Parameters used in the simulation.

Properties	Values	Reference
Margules parameter, A	4800 J/mol	Fitted
Amount of material, w_{MH}	125 mg	Measured
Cell temperature, T	298 K	Measured
Discharge current, j	24 mA/g	Measured
Electrode capacity, Q_o	310 mAh/g	Measured
Exchange current density at 50% SOC, $j_{o,50\%SOC}$	14.24 mA/g	Measured
Particle radius, R_p	5 μm	—
Pellet electrode volume, V	4.5×10^{-2} cm^3	Measured
Porosity, ϵ	0.4	Measured
Reaction orders, p, q	1, 1	—
Reference electrode potential, Φ^o vs. H/HgO	−0.923 V	Measured
Reference hydrogen concentration, c^o	91.3 mol/cm^3	2
Time for diffusion, $t_D = R_p^2/D$	2.4456×10^4 s	Measured
Anodic transfer coefficient, β	0.5	Measured

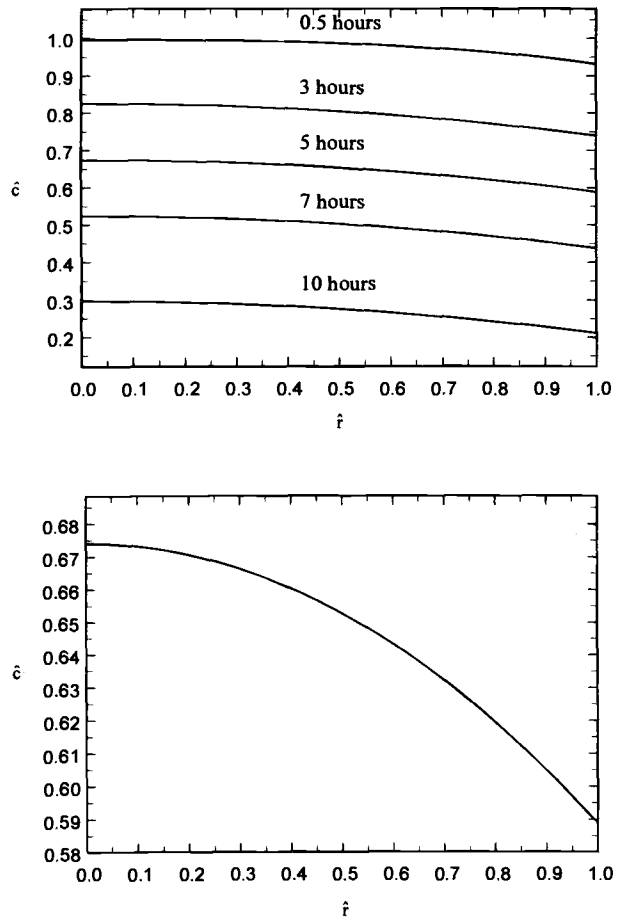

Fig. 2. A plot of the change in dimensionless concentration of hydrogen in the particle at various stages of discharge (a, top). Note that the amount of hydrogen in the particle after 5 h of discharge varies significantly along the radial coordinate (b, bottom).

goes an exponential decay from the bulk of the particle to the surface. When the hydrogen concentration at the surface drops to values close to zero, the electrode potential as given by Eq. 25 changes suddenly to more positive values indicating the end of discharge. The variation in the surface concentration with time for different values of the parameter δ is plotted in Fig. 3. The surface concentration drops exponentially first and then follows a linear decrease with time. The slope of the change in surface concentration with time is controlled by the parameter δ. Increasing the discharge current (increasing δ) results in faster depletion of the active material from the surface.

Exchange current density.—During the polarization studies, the electrode potential was perturbed 20 mV above and below the equilibrium voltage, and the current response was measured at different hydrogen contents. Since the deviation in potential is small, the change in the SOC of the electrode is less than 1%. The linearized form of the Butler-Volmer equation can then be used to calculate the exchange current density, j_o, of the encapsulated alloy

$$j_o = \frac{RT}{FR_{ct}} \qquad [35]$$

Here the charge-transfer resistance denoted by R_{ct} is the slope of the current-potential lines and denotes the extent of change in the electrode potential with current, i.e., the polarizability of the alloy. The exchange current densities for the nickel-plated electrode calculated using Eq. 35 are summarized in Fig. 4 as a function of electrode hydrogen content. Although the concentration of the electroactive species is not explicitly present in Eq. 35, variations in the charge-transfer resistance with hydrogen content as given by Eq. 32 cause j_o to change with the SOC. The dashed line in Fig. 4 is the fit of the experimental data with Eq. 32 using the thermodynamic parameter A as the adjustable parameter. The value of A obtained here has been used in all subsequent simulations. The exchange current is a measure of the system's ability to deliver a net current or a constant potential without a significant energy loss due to activation. From this perspective it is essential that the MH electrode have a constant exchange current density throughout the discharge period. The value of the exchange current density increases, reaches a maximum, remains a constant for most of the discharge, and finally decreases at high SOC as shown in Fig. 4. The exchange current density is also a good measure of the catalytic activity of the electrode for hydrogen evolution/absorption, since j_o is an indication of the height of the free-energy barrier for reaction I at the reversible potential.

Discharge characteristics.—For a constant-current discharge, Eq. 31 was solved for the overpotential using a Newton-Raphson interactive technique. The electrode potential during discharge was determined as a function of the SOC of the electrode as defined by Eq. 34. The constant-current discharge curves at different rates are given in Fig. 5. The discharge curve is characterized by three distinct regions: the activation, mixed, and diffusion-controlled regimes. At the beginning of discharge, the process is under charge-transfer control which is characterized by the initial drop in potential. Subsequently diffusion becomes dominant, and the discharge is under both diffusion and kinetic

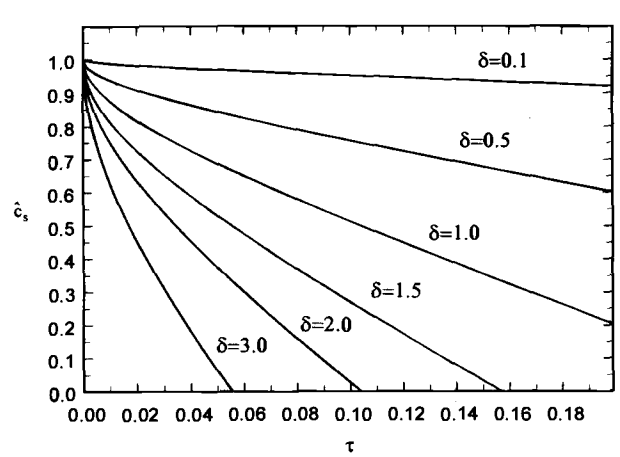

Fig. 3. A plot of the normalized surface concentration of hydrogen as a function of discharge time. Note that the slope of the curve is significantly altered by the value of δ.

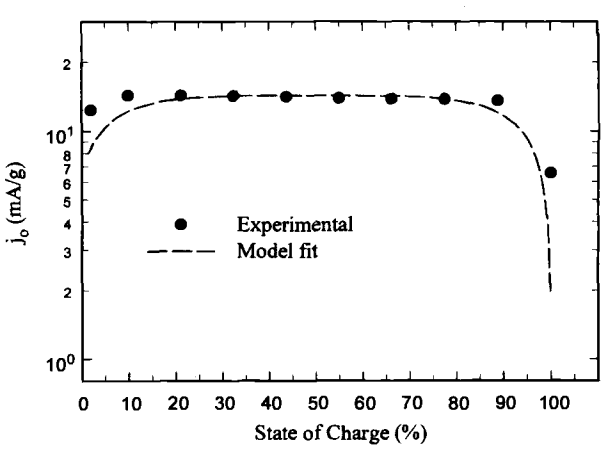

Fig. 4. Plot to obtain the value of the thermodynamic parameters A from experimental discharge current density at different SOC. The best fit was obtained at A = 4800 J/mol which has been used in all subsequent simulations.

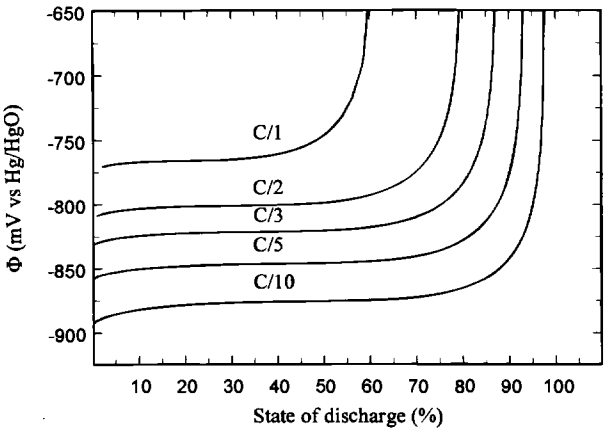

Fig. 5. Simulated discharge profiles of the metal hydride electrode at rates of C/10, C/5, C/3, C/2, and C/1. Note that the increase in discharge rate results in the potential dropping to its cut-off point well before all the hydrogen in the particle has reacted.

control. At the end of discharge the hydrogen concentration is close to zero at the surface, and under these conditions diffusion dominates the desorption reaction. It can be seen that, as the discharge rate increases, the SOC at the end of charge increases. Several investigators[5-11] have explained this behavior in terms of the depletion of atomic hydrogen on the surface of the metal hydride particles. The decrease in the concentration of hydrogen at the surface results in a concentration gradient which induces the diffusion of hydrogen in the metal particle toward the surface. Under high discharge rates, the hydrogen diffusion from the bulk of the hydride alloy to the surface is slow compared to the rate of the electrochemical reaction occurring on the surface of the particles. This reduces the hydrogen concentration to values close to zero and causes the potential to drop before all the hydrogen contained in the particles has reacted.

Figure 6a presents the comparison between the model simulated cell voltage vs. time curves and the experimental data. It can be seen that the model and the experimental data agree very well at two different discharge rates. Both the model predictions and the experimental results indicate that the electrode voltage drops quickly from the initial potential to more positive values at the beginning of discharge, then decays very slowly during the main course of discharge, and finally falls off upon complete discharge. The discharge profile for 34 mA/g neglecting the hydrogen-metal interactions (A = 0) is presented in Fig. 6b. As seen from the plot, the electrode potential changes continuously during discharge, and the plateau observed in the experimental discharge curve is completely absent. These results indicate that the changes in the interactions between the hydrided and bare alloy significantly affect the alloy performance.

The simultaneous effects of the hydrogen diffusion in the bulk of the alloy and the reaction on the hydride surface need to be optimized to enhance the performance of the hydride electrode. Figure 7 shows the effect of the exchange current density on the discharge curves. The exchange current density at 50% SOC is varied, and the potential response is simulated. Decreasing the exchange current results in increasing initial drop in potential as seen in Fig. 7. Hence, the overpotential given by the difference in the electrode and equilibrium potentials increases with decreasing values of the reaction rate. Therefore for practical systems, alloys with high $j_{o,ref}$ are preferred. The time at which the electrode potential drops rapidly to more positive values indicates that the electrode has been completely discharged. From Fig. 7, we can see that the time for complete discharge of the electrode remains the same for all values of the exchange current. These results indicate that the utilization of the electrode remains unaffected with changes in the reaction rate at the surface. However, the reaction rate contributes significantly to the polarization losses and affects the energy density of the electrode. The electrode utilization and capacity are determined by the diffusion limitations of the alloy.

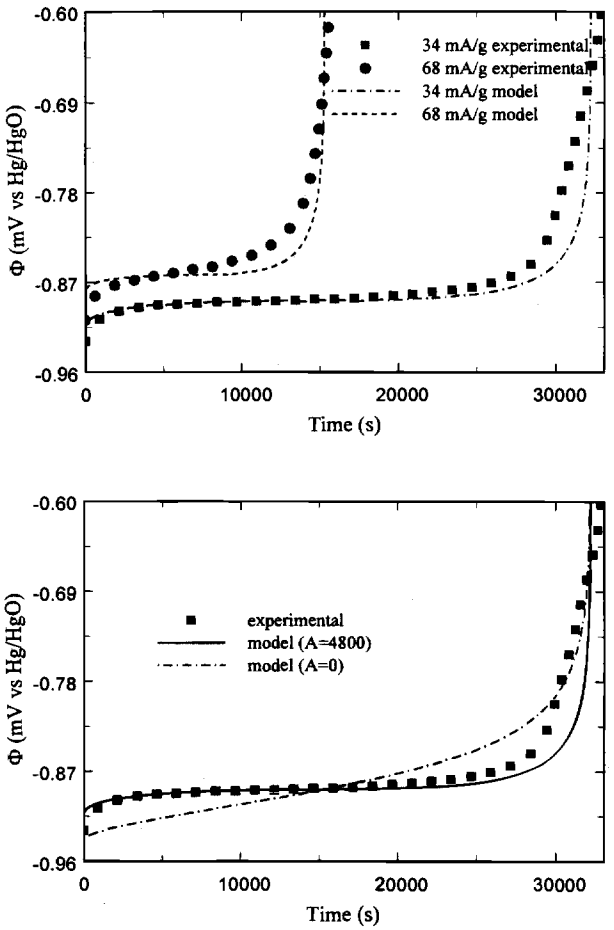

Fig. 6. Comparison of the experimental data and theoretical discharge potential at two different discharge rates (a, top) for an alloy weight of 0.144 g. The model considering the hydrogen-metal site interactions predicts a potential plateau during most of the discharge. Neglect of the changes in the activity coefficients results in predictions (A = 0) where the potential varies during the entire duration of discharge (b, bottom).

We define a dimensionless parameter, ν, relating the time for discharge under ideal conditions to the time for transport of hydrogen in the alloy

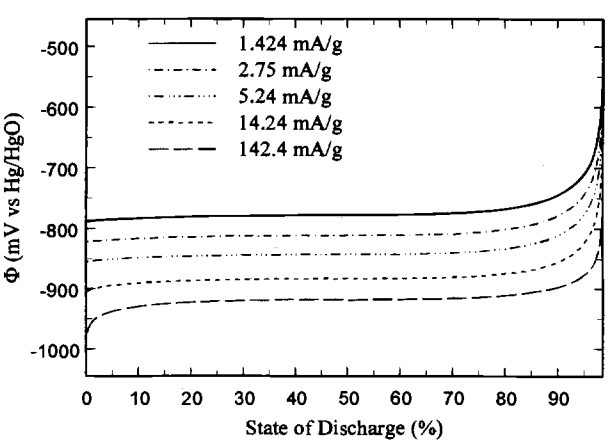

Fig. 7. Effect of the reaction resistance on the discharge profiles of the hydride electrode. Note that varying the exchange current density has no effect on the final time for complete discharge of the electrode. However, the polarization losses of the electrode decrease with the lowering of the reaction resistance.

$$\nu = \frac{3600 Q_o D}{j R_p^2} \quad [36]$$

where j represents the current used to determine the actual capacity of the electrode (24 mA/g in our case). Discharge curves for different values of the parameter ν are shown in Fig. 8. It is seen that the effect of decreasing the diffusion coefficient affects the electrode behavior in the same way as increasing the discharge rate. The two parameters, the discharge rate and the diffusion coefficient are interrelated because at high discharge rates, hydrogen diffusion from the bulk of the hydride will be slow compared to the rate of the electrochemical reaction occurring on the surface of the particles. Similarly, the discharge time decreases, and the utilization of the electrode is lower with a decrease in the rate of hydrogen diffusion. A similar effect can also be achieved by increasing the particle size of the alloy. Hence, for a given discharge rate, depending on the value of the diffusion coefficient and the particle size, the charge left in various hydride alloys will be different at the end of discharge.

For practical applications of hydrides, the parameter of interest is the electrode utilization. Figure 8 shows that the discharge time is sensitive to changes in ν and a decrease in one order of magnitude of this parameter from 0.47 to 0.047 results in reducing the electrode utilization by 60%. The parameter R_p^2/D is the time for diffusion, t_D, and represents the discharge time of the electrode if it is under diffusion control only. Figure 9 shows the utilization of the electrode as given by Eq. 16 for different values of the time for discharge. In actual hydride electrodes the pulverization effect results in reducing the particle size of the alloy to approximately 10 to 15 μm.[20] With a t_D of the order of 10^5 s, this gives a value of diffusion coefficient of approximately 10^{-11} cm^2/s. The diffusion coefficient of hydrogen in the alloy is determined by the alloy constituents and can be modified by different substitutions.[21] The diffusion coefficient in a given charge-discharge cycle varies due to the α-β transitions.[22] For an alloy of given material, the diffusion coefficient does not change significantly with cycling. However, the particle size varies considerably during charge-discharge cycles, and this would affect the utilization of the electrode significantly. Hence design of hydride electrodes needs to focus on optimizing the particle size during cycling.

Equilibrium potential.—The potential of the nickel plated electrode on immersion initially in the 6 M KOH solution was −0.552 V. Once the electrode was charged, the potential reached more negative values because of the hydrogen intake. After activation, the SOC studies were done once the electrode potential at the end of discharge had stabilized. Using the three-electrode setup, the constant equilibrium potential at different values of hydrogen content was measured with respect to the Hg/HgO reference electrode.

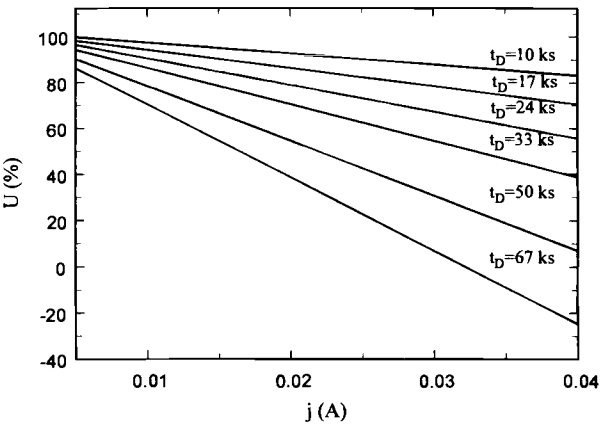

Fig. 9. Effect of the time for diffusion on the utilization of the hydride electrode. Note that, for a constant diffusion coefficient, varying the particle size significantly affects the electrode utilization.

Yayama et al.[12,13] presented comparisons between the experimental and predicted equilibrium potential at low states of charge for a $TiMn_{1.5}H_x$ alloy. Expressions employed for the equilibrium potential in their analysis had a reaction-order dependence on the concentration of hydrogen. However, the equilibrium potential is a purely thermodynamic parameter and does not depend on the reaction orders which are related to the kinetics of the interface processes. Figure 10 presents a comparison of the experimental equilibrium potentials for the nickel-plated electrode with the simulated values as given by Eq. 25. The electrode potential at equilibrium shows the thermodynamic limit of reversibility and the maximum energy density obtainable from the cell under no kinetic and ohmic limitations. As seen from the plot, the equilibrium potential changes to more negative values with an increase in the hydrogen concentration in the alloy. Except at high and low SOC values, the potential values remain approximately the same. Upon completely charging the electrode, most of the vacant sites on the surface of the particle have been filled. When the surface concentration ($\hat{c}_s$) becomes 0 or 1, the potential as given by Eq. 25 tends to $+\infty$ and $-\infty$, respectively. This is similar to what we observe experimentally. At a low state of charge (SOC), due to the depletion of hydrogen at the surface, a sudden drop in the potential toward more positive values is seen. Similarly at high SOC, again a drop to more negative potentials is seen. The model predicts the drop in the potential in both these cases. The mathematical limits of $+\infty$ and $-\infty$ represent these two extremes. The constant potential for most SOC

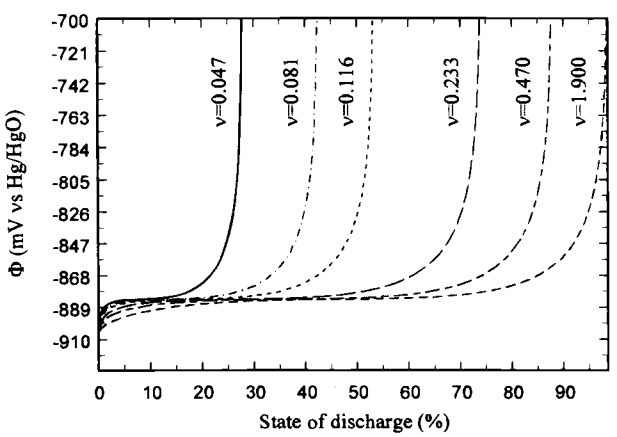

Fig. 8. Simulated profiles of the electrode potential for different values of the parameter ν. Note that the effect on the electrode behavior of ν is similar to that of the discharge rate as shown in Fig. 5.

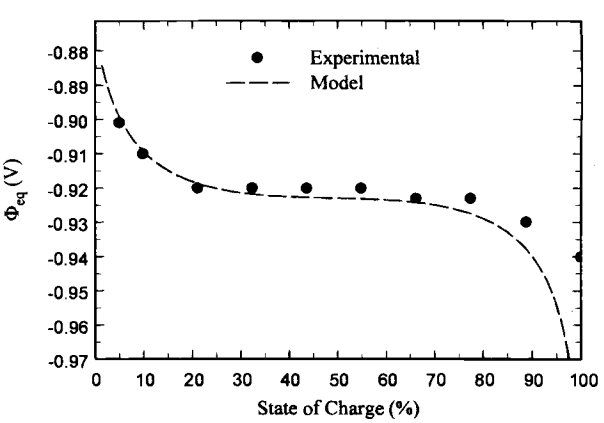

Fig. 10. Comparison of model predictions and experimental values of the electrode equilibrium potential at different SOC. The equilibrium potential varies at low and high SOC due to changes in the hydrogen and metal site concentration, respectively.

values arises due to the interactions between the bare and hydrided alloy phases.

Conclusions

An analytic model for the discharge of the hydride electrode under galvanostatic conditions was developed. A theoretical formalism for predicting the thermodynamic and kinetic parameters of the hydride electrode has been outlined. The Butler-Volmer equation for the reaction at the surface of the alloy was derived considering the hydrogen-metal site reactions. The discharge model and the different equations derived are general in nature and can be used for any hydride material. The analytic model coupled with the Margules thermodynamic correction for the activity coefficients was used to study the hydride electrode under different conditions. The interaction parameter A was found to alter significantly the shape of the predicted discharge curves. Experimental discharge curves reveal a potential plateau during most part of the discharge. Neglecting the activity-coefficient variations with concentration ($A = 0$) resulted in discharge curves which differed significantly from the actual physical process. General battery models of the Ni-MH cells could incorporate the equilibrium equations developed in this paper in order to get better estimates of the discharge potential. The effect of an increase in the reaction resistance at the surface of the alloy results in a rise in the polarization losses of the electrode. Model simulations indicate that diffusional resistance forms the major contributor to the electrode polarization. The electrode utilization was found to be sensitive to changes in the time for diffusion. The particle size of the alloy and the hydrogen diffusion coefficient were found to be the determining factors of the electrode utilization. Thermodynamic and kinetic data critical to the optimization of the electrode performance have also been simulated. An analysis of the equilibrium potential reveals the change in the open-circuit potential of the alloy with state of charge. Comparison of simulations of these parameters with experimental data reveals good agreement.

Acknowledgment

Financial support by the Exploratory Technology Research Program, which is supported by the Office of Transportation Technologies of the U.S. Department of Energy, subcontract no. 4614610, is acknowledged gratefully.

Manuscript submitted November 19, 1997; revised manuscript received July 20, 1998.

The University of South Carolina assisted in meeting the publication costs of this article.

LIST OF SYMBOLS

$\hat{a}_H$	dimensionless activity of adsorbed hydrogen
$\hat{a}_M$	dimensionless activity of metal sites
a_{MH}	electroactive surface area per unit volume of electrode, cm^2/cm^3
A	symmetrical Margules interaction parameter, J/mol
c	concentration of hydrogen, mol/cm^3
c^o	reference hydrogen concentration, mol/cm^3
$\hat{c}$	dimensionless hydrogen concentration, c/c^o
$\bar{c}$	dimensionless average concentration of hydrogen in a particle
$\hat{c}_s$	dimensionless surface concentration of hydrogen
D	diffusion coefficient of hydrogen, cm^2/s
f	F/RT, 38.94 V^{-1}
F	Faraday's constant, 96,487 C/mol
G_E	excess free energy, J/mol
G_I	free energy of mixing, J/mol
G_R	free energy of reaction, J/mol
G_T	total free energy, J/mol
j	specific discharge current, A/g of active material
j'	local current density, A/cm^2
j_o	concentration dependent exchange current density, A/cm^2
$j_{o,ref}$	reference exchange current density, A/cm^2
$j_{o,50\%\ SOC}$	experimentally measured exchange current density at 50% SOC, A/g
k_+, k_-	reaction rate constants, $s^{-1}\ cm^{-2}$
p	hydrogen reaction order
q	metal site reaction
Q_o	specific capacity of the electrode, Ah/g of active material
r	radial coordinate, cm
$\hat{r}$	dimensionless radial coordinate, r/R_p
R_p	radius of the metal hydride particles, cm
R	universal gas constant, 8.314 J/mol-K
t	time, s
T	temperature, K
U	electrode utilization
V	volume of the cylindrical pellet electrode, cm^3
w_{MH}	amount of active material, g

Greek

β	anodic transfer coefficient
δ	dimensionless parameter denoting ratio between diffusional and kinetic resistances, $j'R_p/Fc^oD$
ϵ	porosity of the electrode
η	overpotential, V
γ	activity coefficient
λ_n	root of $\tan \lambda_n - \lambda_n = 0$, $n = 1, 2, ..\infty$
μ	standard chemical potential, J/mol
ν	dimensionless parameter denoting ratio between the ideal time for discharge to the time for diffusion, $3600Q_oD/IR_p^2$
Φ	electrode potential difference at the interface, V
Φ_{eq}	hydride equilibrium potential, V
Φ^o	standard hydride equilibrium potential at 50% SOC, V
τ	dimensionless time, tD/R_p^2
τ_d	dimensionless time to discharge the electrode completely, R_p^2/D

Subscripts

H	adsorbed hydrogen
M	unhydrided alloy

Superscripts

o	reference standard state

REFERENCES

1. G. Sandrock, in *Proceedings of the Symposium on Hydrogen and Metal Hydride Batteries*, P. D. Bennett and T. Sakai, Editors, PV 94-27, p. 219, The Electrochemical Society Proceedings Series, Pennington, NJ (1994).
2. T. H. Fuller and J. Newman, in *Modern Aspects of Electrochemistry*, Vol. 27, R. E. White, J. O'M. Bockris, and B. E. Conway, Editors, p. 359, Plenum Press, New York (1993).
3. H. F. Bittner and C. C. Badcock, *J. Electrochem. Soc.*, **130**, 193C (1983).
4. M. Viitanen, *J. Electrochem. Soc.*, **140**, 936 (1993).
5. M. H. J. Van Rijswick, in *Hydrides for Energy Storage*, A. F. Andresen and A. J. Maeland, Editors, p. 261, Pergamon Press, Oxford (1978).
6. Q. M. Yang, M. Ciureanu, D. H. Ryan, and J. O. Strom-Olsen, *J. Electrochem. Soc.*, **141**, 2111 (1994).
7. B. Paxton and J. Newman, *J. Electrochem. Soc.*, **144**, 3818 (1997).
8. B. E. Conway and J. Wojtowicz, *J. Electroanal. Chem.*, **326**, 277 (1992).
9. J. Heikonen, K. Vuorilehto, and T. Noponen, *J. Electrochem. Soc.*, **143**, 3972 (1996).
10. A. Lasia and D. Gregoire, *J. Electrochem. Soc.*, **142**, 3393 (1995).
11. P. De Vidts, J. Delgado, and R. E. White, *J. Electrochem. Soc.*, **142**, 4006 (1995).
12. H. Yayama, K. Hirakawa, and A. Tomokiyo, *Jpn. J. Appl. Phys.*, **25**, 739 (1986).
13. H. Yayama, K. Kuroki, K. Hirakawa and A. Tomokiyo, *Jpn. J. Appl. Phys.*, **23**, 1619 (1984).
14. Q. M. Yang, M. Ciureanu, D. H. Ryan, and J. O. Strom-Olsen, *Electrochim. Acta*, **40**, 1921 (1995).
15. W. Zhang, S. Srinivasan, and H. J. Ploehn, *J. Electrochem. Soc.*, **143**, 4039 (1996).
16. H. S. Carslaw and J. C. Jaeger, *Conduction of Heat in Solids*, Oxford University Press, London (1973).
17. R. Barnard, C. F. Randell, and F. L. Tye, *J. Appl. Electrochem.*, **10**, 127 (1980).
18. M. W. Verbrugge and B. J. Koch, *J. Electrochem. Soc.*, **143**, 600 (1996).
19. M. Jain, A. L. Elmore, M. A. Mathews, and J. W. Weidner, *Electrochim. Acta*, Submitted.
20. G. Zheng, B. N. Popov, and R. E. White, *J. Electrochem.*

Soc., **142**, 2695 (1995).
21. R. C. Bowman, Jr., B. D. Craft, A. Attalla, M. H. Mendelsohn, and D. M. Gruen, *J. Less-Common Met.*, **73**, 227 (1980).
22. P. Fischer, A. Furrer, G. Busch, and L. Schlapbach, *Helvet. Phys. Acta*, **50**, 421 (1977).

Nucleation and Growth of Zinc from Chloride Concentrated Solutions

G. Trejo, R. Ortega B.,* and Y. Meas V.

Centro de Investigación y Desarrollo Tecnológico en Electroquímica, Parque Tecnológico Querétaro-Sanfandila, Pedro Escobedo, Qro. México 76700

P. Ozil, E. Chainet, and B. Nguyen

Laboratoire d'Electrochimie et Physicochimie de Matériaux et Interfaces, Ecole Nationale Supérieure d'Electrochimie et d'Electrometallurgie de Grenoble, Saint Martin d'Heres, Cedex 38402, France

ABSTRACT

The electrodeposition of metals is a complex phenomenon influenced by a number of factors that modify the rates of nucleation and growth and determine the properties of the deposits. In this work we study the influence of the zinc chloride ($ZnCl_2$) concentration on the zinc nucleation process on glassy carbon, in a KCl electrolyte under conditions close to those employed in commercial acid deposition baths for zinc. The electrochemical study was performed using cyclic voltammetry and potentiostatic current-time transients. The charge-transfer coefficient and the formal potential for $ZnCl_2$ reduction were evaluated from cyclic voltammetry experiments. The nucleation process was analyzed by comparing the transients obtained with the known dimensionless $(i/i_m)^2$ vs. t/t_m reponse for instantaneous or progressive nucleation. The results show that the nucleation process and the number density of sites are dependent on $ZnCl_2$ concentration. Scanning electron microscopy analysis of the deposits shows that the deposits are homogeneous and compact although a change in the morphology is observed as a function of $ZnCl_2$ concentration. Evaluation of the corrosion resistance reveals the influence of the nucleation process on the subsequent corrosion resistance of the zinc deposits.

Introduction

Electrodeposition of zinc and its alloys has been widely implemented as a corrosion resistant coating on steel. The coating cathodically protects the steel from the environment. Considerable research has been conducted on the factors affecting the quality of the electrodeposits, e.g., crystallographic orientation, nature of the substrate, additives, composition, etc.[1-3] For the electroplating of zinc on glassy carbon at low overpotentials from solutions containing 3 M $ZnCl_2$ or 3 M $ZnBr_2$, McBreen and Gannon[4] showed that the nucleation overpotential is smaller for $ZnCl_2$ than for $ZnBr_2$ solution probably due to the lower stability constant of $ZnBr_2$. In both systems nucleation was observed to proceed instantaneously with subsequent growth being controlled by diffusion. In another study the nucleation rate and number density of active sites for zinc electrodeposition from zinc chloride in a sodium chloride supported electrolyte was found to increase with chloride concentration.[5]

The type of nucleation and the deposition kinetics are sensitive to the presence of impurities as well as of organic and inorganic additives at low concentrations. In a general way, additives modify the deposition overpotential and change the rate of nucleation and growth.[6-8] For example the presence of small particles of ammonium chloride in the baths containing zinc chloride reduces the costs and improves the quality of the obtained deposits.[9] The substrate is another factor known to modify the nucleation mechanism as shown by studies of zinc deposition on Pt, Au, and graphite electrodes.[10] Similarly nucleation may be influenced by applying an alternating current. This has been shown to improve the homogeneity of the deposits.[11]

Although zinc electrodeposition has been widely studied, few works[12] have focused on the relationship between film growth, i.e., nucleation, morphology, etc., and the resistance against corrosion.

This work is devoted to the study of the electrochemical deposition of zinc on glassy carbon (GC) from concentrated KCl solutions. Because the high overpotential for the hydrogen evolution reaction on glassy carbon, this substrate allows the study of zinc deposition without the interference of the hydrogen evolution reaction. The $ZnCl_2$ concentrations were selected within the range of the concentrations generally used in the commercial acid baths for zinc deposition.[13-15] Voltammetry, chronoamperometry, and scanning electron microscopy (SEM) studies were carried out to determine the nucleation growth mechanism of zinc deposition for different $ZnCl_2$ concentrations. Subsequent analysis lead us to propose a relationship between nucleation mechanism, morphology, and sacrifical protective power of zinc deposits on steel.

Experimental

Zinc was electrochemically deposited from solutions containing $ZnCl_2$ (Merck) at different concentrations (0.01, 0.1, 0.2 , 0.3, 0.4, and 0.6 M) in 2.8 M KCl (Merck). The pH was adjusted to 5.0 by adding 0.1 M HCl. The solutions were prepared with triply distilled, deionized (18 MΩ cm) water. All reagents were analytical grade.

The electrochemical experiments were performed in a conventional three-electrode cell with a water jacket. The working electrode was a glassy carbon disk (GC) (0.07 cm^2 geometric surface area); a saturated calomel electrode (SCE) (Tacussel) was used as the reference electrode, and all potentials in this work are referred to it. A graphite rod was used as counter electrode. Prior to each experiment, the working electrode was polished with alumina 0.05 mm (Buehler) and electrochemically pretreated in a solution containing 0.01 M $K_4Fe(CN)_6$ and 1 M KNO_3. All experiments were performed under ultrapure nitrogen atmosphere (Linde).

Corrosion evaluation of zinc coated AISI 1018 steel was performed on electrodes with a 1 cm^2 geometric surface area that were isolated in epoxy resin rods. The experiments were carried out in 3.5% NaCl solution which was aerated by bubbling with ultrapure oxygen (Linde) for 1 h prior to use.

* Electrochemical Society Active Member.